Protective Coating of Superparamagnetic Iron Oxide Nanoparticles

Do Kyung Kim,* Maria Mikhaylova, Yu Zhang, and Mamoun Muhammed

Materials Chemistry Division, Royal Institute of Technology, SE-100 44 Stockholm, Sweden

Received November 5, 2002. Revised Manuscript Received February 19, 2003

Magnetic nanoparticles are becoming increasingly important for several biomedical applications. For example, superparamagnetic magnetite nanoparticles with suitable biocompatible coatings are useful in magnetic resonance imaging, tissue engineering, and drug delivery, etc. In this study we report the synthesis of magnetite nanoparticles and the further coating of these particles by several types of protective layers. Thermodynamic modeling of the chemical system has been adopted as a rational approach to establish routes to better synthesis conditions for pure phase magnetite. Quantitative analysis of different reaction equilibria involved in the precipitation of magnetite from aqueous solutions has been used to determine optimum synthesis conditions. Superparamagnetic magnetite nanoparticles (SPION) with diameters of 6 and 12 nm have been prepared by controlled chemical coprecipitation of magnetite phase from aqueous solutions containing suitable salts of Fe^{2+} and Fe^{3+} under inert atmosphere. Pure magnetite phase SPION could be observed from X-ray diffraction. Magnetic colloid suspensions containing particles with three different types of coatings (sodium oleate (NaOl), starch, and methoxypoly(ethylene glycol) (MPEG)) have been prepared by using different stabilization methods. SPION coatings were studied by determining the change of the surface charge by electrokinetic sonic amplitude (ESA) measurements, as a function of varying NaOl in the solution, where the amount of NaOl needed to form a stable suspension was determined. For stable suspension, the optimum concentration of sodium oleate (NaOl) chemisorbed at 2.5 g of SPION surface is 5.2×10^{-7} M NaOl which shows maximum ESA value of 0.034 mPa•M/V. SPION coating by starch results in the formation of agglomerate. The agglomeration size of starch-coated SPION can be decreased by introducing H_2O_2 as an oxidizing agent; the resulting particle size is 42 nm as determined by dynamic light scattering (DLS). For the modification of SPION surfaces with MPEG, the surface was first silanized by 3-aminopropyltrimethoxy silane (APTMS) as a coupling agent with a thickness of two or three molecular layers. AFM image shows that each cluster includes several magnetite single particles with the cluster size around 120 nm. SPION, both coated and uncoated, have been characterized by several techniques. AFM was used to image the MPEG-coated SPION. FTIR study indicated that the different coating agents cover the SPION surface. Magnetic characterization was carried out using SQUID and Mössbauer spectroscopy.

Introduction

Nanoparticles have attracted the attention of an increasing number of researchers from several disciplines during the past decade. The term "nanoparticle" is generally used in materials science to specify particles with diameters less than 100 nm. Nanotechnology is the utilization of structures and devices with a size range from ∼1 (molecular scale) to ∼50 nm where the physical, chemical, and biological properties are significantly enhanced/changed or completely different from those of the corresponding bulk materials.[1]

Synthesis and processing of nanoparticles with controlled properties, such as chemical (composition of the bulk, interaction between the particles, and surface charge) and structural (crystalline or amorphous, size, and morphology) characteristics, are the main features for the design of nanoobjects (nanoparticles/nanotubes/nanolayers) for specific applications. The development of supramolecular, biomolecular, and dendrimer chemistries for engineering substances on the ångström and nanoscale dimensions has been the focus of interest in nanotechnology. The emerging disciplines of nanoengineering, nanoelectronics, and nanobioelectronics require suitably sized functional building blocks to construct complex architectures and devices.[2]

Magnetic nanoparticles (MP) have been extensively studied because of their potential application in several areas, including in-vitro cell separation,[3] in-vivo drug delivery,[4] immunoassay,[5] immunomagnetic array,[6] mag-

* To whom correspondence should be addressed. E-mail: kyung@matchem.kth.se or mamoun@matchem.kth.se.

(1) Schoonman, J. *Solid State Ionics* **2000**, *135*, 5.

(2) (a) Edelstein A. S.; Cammarata, R. C. *Nanomaterials: Synthesis, Properties and Applications*; Institute of Physics Publishing: London, 1998. (b) Ikai, A. *Superlatt. Microstruct.* **2002**, *31*, 43. (c) Cohen, M. L. *Mater. Sci. Eng. C* **2001**, *15*, 1. (d) Chová, T.; Guttman, A. *Trends Biotechnol.* **2002**, *20*, 116.

10.1021/cm021349j CCC: $25.00
Published on Web 03/22/2003

netic storage,[7] MR contrast agent,[8,9] magnetic ink printing,[10] and microwave absorption.[11]

Several different types of magnetic micro- and nanoparticles and magneto bacteria are developed for biomedical applications.[12] For in vitro application, biologically active compounds have been immobilized on MP and can be easily isolated or moved from a basic solution such as blood, bone marrow, or tissue to the target by applying an external magnetic field.[13]

Immunomagnetic separation (IMS) is more commonly used in the isolation of cells using a single parameter.[14] Magnetic separation methods using positive selection (i.e., enrichment of cells of interest) and negative selection (i.e., depletion of unwanted cells) are possible.[15] Partington et al.[16] described IMS based on a dual parameter sorting technique involving two-stage immunomagnetic selections which permits isolation of cells based on a second cell surface marker without the need for the removal of beads used in the first selection step. Bildirici et al.[17] used silica beads for separating cells by comparing magnetic beads for density perturbation by measuring their affinity and modification of target cells. Generally, magnetically assisted assays are relatively faster and more reproducible than the standard microtitration plate-based assays. In a study by Suzuki et al.,[18] MP with immobilized anti-mouse IgG antibody or protein A were used for enzyme-linked immunosorbent assay (ELISA) of mouse IgG. The assay time was substantially shorter than the conventional method.

Superparamagnetic iron oxide nanoparticles (SPION) were recently introduced as a suitable material for MR imaging, drug delivery, drug-targeting, and hyperthermia agent through intravenous or extravenous injection.[4,8,9] Especially for MR imaging purposes, imaging agents are required to increase conspicuity of adjacent internal organs and tissue.[9] Moreover, SPION can be used to monitor extracellular macromolecules both at a single cell level (genes and proteins) and at a network level (intercellular communication) by in-vivo monitoring of particle movement in the living brain tissue. For example, in the first stage of a tumor, it is difficult to distinguish when using only MR imaging because of the limited sensitivity of the MRI equipment. However, the signal intensity of MRI can be improved by introducing SPION as a contrast agent. Moreover, an external drag force can be applied to move the surface-modified SPION to a target tissue. Another way to move the SPION is through the modification of their surfaces with a specific functional group that can specially interact with the target tumor/cancer.[19−21]

When the particle size of iron oxide is larger than 50 nm, it can be used mainly for in vitro magnetic separation purposes due to its ferromagnetic behaviors. As an example, in-vivo biomedical applications for neuro research using SPION require particle size less than 50 nm, which is the diameter of the reticuloendothelial system (RES) in the brain, where the particles should have a narrow size distribution and surface coating with biocompatible materials, i.e., nonimmunogenic, nonantigenic, and protein-resistant. To transport this hydrophilic substance in a biological membrane system, surface modifications of the nanoparticles are necessary to adjust the ξ-potential close to zero at pH = 7.4.

For a stable dispersion, forces due to thermal motion, repulsion, etc. in the ferrofluid must be stronger than the attraction forces in order to stabilize as a ferrofluid. The stability of ferrofluids composed of SPION are not only affected by an inhomogeneous particle size distribution, but are also affected by the surface charge of the particles in the solution. One practical method to stabilize the ferrofluid is through electrostatic stabilization, achieved by the electrostatic repulsion of similarly charged surfaces. The repulsive force results from creation of an electric double layer around the particles, which is dependent on dispersion of the particles into a polar media, pH, concentration, and ionic strength of the suspension.

Three different types of magnetic colloids can be prepared through various stabilization methods (Figure 1). The first magnetic colloid is prepared by coating a magnetic core with a suitable surfactant, e.g., sodium oleate (NaOl) on SPION.[22] The second stabilization method is based on the formation of nanocomposites consisting of SPION distributed throughout grafting a nonmagnetic coating, e.g. polymeric starch. The presence of polymeric starch during the formation of SPION hinders cluster growth after nucleation. These polymeric networks cover a large number of continuously formed iron oxide monodomains and hold them apart against attracting forces by surface tension. In addition, the formation of a polymer layer on the surface of the magnetite nanoparticles prevents further oxidation,

(3) (a) Begg, A. C.; Sprong, D.; Balm, A.; Martin, J. M. C. *Radiother. Oncol.* **2002**, *62*, 335. (b) Sieben, S.; Bergemann, C.; Lübe, A.; Brockmann, B.; Rescheleit, D. *J. Magn. Magn. Mater.* **2001**, *255*, 175.

(4) Roullin, V. G.; Deverre, J. R.; Lemaire, L.; Hindré, F.; Julienne, M. C. V.; Vienet, R.; Benoit, J. P. *Eur. J. Pharm. Biopharm.* **2002**, *53*, 293.

(5) (a) Mura, C. V.; Becker, M. I.; Orellana, A.; Wolff, D. *J. Immuno. Methods* **2002**, *260*, 263. (b) Tanyolac, D.; Özdural, A. R. *React. Funct. Polym.* **2000**, *43*, 279. (c) Roitt, I. *Essential Immunology*; Blackwell Scientific Publications: London, 1994.

(6) Call, D. R.; Brockman, F. J.; Chandler, D. P. *Int. J. Food Microbiol.* **2001**, *67*, 71.

(7) Chakraborty, A. *J. Magn. Magn. Mater.* **1999**, *204*, 57.

(8) (a) Kim, D. K.; Zhang, Y.; Voit, W.; Rao, K. V.; Kehr, J.; Bjelke, B.; Muhammed, M. *Scr. Mater.* **2001**, *44*, 1713. (b) Wunderbaldinger, P.; Josephson, L.; Weissleder, R. *Bioconjugate Chem.* **2002**, *13*, 264. (c) Jung, C. W.; Jacobs, P. *Magn. Reson. Imaging* **1995**, *13*, 661.

(9) Kim, D. K.; Zhang, Y.; Kehr, J.; Klason, T.; Bjelke, B.; Muhammed, M. *J. Magn. Magn. Mater.* **2001**, *255*, 256.

(10) Peikov, V. T.; Jeon, K. S.; Lane, A. M. *J. Magn. Magn. Mater.* **1999**, *193*, 307.

(11) Pinho, M. S.; Gregori, M. L.; Nunes R. C. R.; Soares, B. G. *Polym. Degrad. Stab.* **2001**, *73*, 1.

(12) (a) Matsunaga T.; Takeyama, H. *Supramol. Sci.* **1998**, *5*, 391. (b) Slocik, J. M.; Moore, J. T.; Wright, D. W. *Nanoletters* **2002**, *2*, 169.

(13) Prestvik, W. S.; Berge, A.; Mørk, P. C.; Stenstad, P. M.; Ugelstad, J. In *Scientific and Clinical Applications of Magnetic Carriers*; Häfeli, U., Schütt, W., Teller, J., Zborowski, M., Eds.; Plenum Press: New York and London, 1997; p 457.

(14) Papadimitriou, C. A.; Roots, A.; Koenigsmann, M.; Koenigsmann, M.; Mucke, C.; Oelmann, E.; Oberberg, D.; Reufi, B.; Thiel, E.; Berdel, W. E. *J. Hematother.* **1995**, *4*, 539.

(15) Anderson, G.; Owen, J. J. T.; Moore, N. C.; Jenkinson, E. J. *J. Immunol.* **1994**, *153*, 1915.

(16) Partington, K. M.; Jenkinson, E. J.; Anderson, G. *J. Immuno. Methods* **1999**, *223*, 195.

(17) Bildirici, L.; Rickwood, D. *J. Immunol.* **2001**, *252*, 57.

(18) Suzuki, M.; Kamihira, M.; Shiraishi, T.; Takeuchi, H.; Kobayashi, T. *J. Ferment. Bioeng.* **1995**, *80*, 78.

(19) Gautherie, M. *Biological Basis of Oncologic Thermotherapy*; Springer: Berlin, 1990.

(20) Hand, J. *Physical Techniques in Clinical Hyperthermia*; Wiley: New York, 1986.

(21) Vrba, J.; Lapeš, M. *Microwave Applicators for Medical Applications*; CVUT Press: Prague, 1997.

(22) (a) Kim, D. K.; Zhang Y.; Voit, W.; Rao, K. V.; Muhammed, M. *J. Magn. Magn. Mater.* **2001**, *225*, 30. (b) Kim, D. K. Ph.D. Thesis, Royal Institute of Technology, Stockholm, 2002.

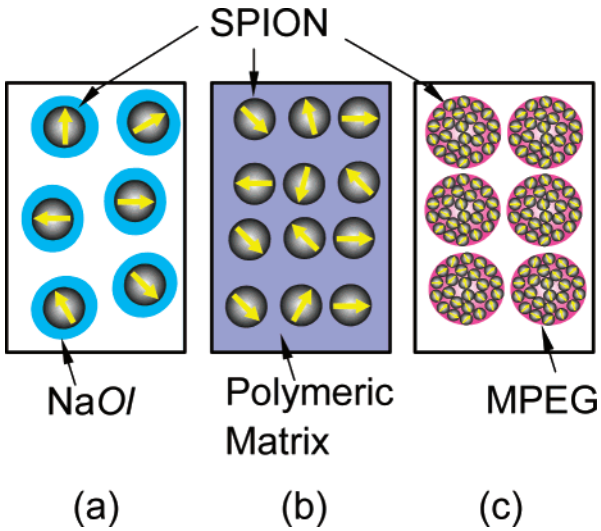

Figure 1. Schematic representation of three types of magnetic colloids: (a) small (typically ~12 nm) core−shell structure magnetite nanoparticles in which magnetic dipole−dipole interactions are screened by a layer of NaOl; (b) prepared in polymeric matrix with a primary agglomeration size 36 nm; and (c) MPEG-modified SPION (primary agglomeration 120 nm).

which affects phase transformation. The third magnetic colloid suspension is stabilized, in a manner similar to that of starch, by MPEG immobilization on the SPION surface.[23]

The particular interest in this work is the design and fabrication of bio-active and bio-compatible multifunctionalized SPION with diameter less than 20 nm after grafting with biocompatible molecules for successful transport of immunomagnetic SPION through biological membranes. The surface modification parameters have been considered for stable suspensions in physiologically compatible solutions such as CSF and in proper carrier matrix or stabilizing agents.

Experimental Section

1. Chemicals and Materials. All chemicals were of reagent grade and used without further purification. Ferric chloride hexahydrate ($FeCl_3 \cdot 6H_2O$, >99%), ferrous chloride tetrahydrate ($FeCl_2 \cdot 4H_2O$, >99%), and starch (25−30 KDa, $(C_6H_{10}O_5)_n$, >99%) were obtained from Aldrich. Hydrogen peroxide (H_2O_2, >99%) and hydrochloric acid (HCl, >37%) were obtained from KEBO. Cationic starch (from potato, 25−30 KDa $(C_6H_{10}O_5)_n$), sodium oleate (anionic surfactant, NaOl, $CH_3(CH_2)_7CH{=}CH(CH_2)_7COONa$), and methoxypoly(ethylene glycol) 5000 (MPEG, $CH_3{-}(OCH_2CH_2)_n{-}OH$) were obtained from Sigma. The potato starch contained quaternary ammonium groups (2-hydroxy-3-trimethylammonium-propyl starch) and its degree of substitution (DS) was 0.352. Milli-Q water was re-deionized (specific conductance <0.1 s/cm) and deoxygenated by bubbling with N_2 gas for 1 h prior to use.

2. Preparation of Magnetic Colloid. The chemical reaction of Fe_3O_4 precipitation is given by

$$Fe^{2+} + 2\ Fe^{3+} + 8\ OH^- \rightarrow Fe_3O_4 + 4\ H_2O \qquad (1)$$

According to the results of thermodynamic modeling of this system, a complete precipitation of Fe_3O_4 is expected in the pH range 7.5−14 while maintaining a molar ratio of Fe^{2+}/Fe^{3+} = 1:2 under a non-oxidizing environment. Under oxidizing conditions, Fe_3O_4 may be oxidized as given by the following equations.

$$Fe_3O_4 + 0.25\ O_2 + 4.5\ H_2O \rightarrow 3\ Fe(OH)_3 \qquad (2)$$

$$Fe_3O_4 + 0.25\ O_2 \rightarrow 1.5\ Fe_2O_3 \qquad (3)$$

Aqueous dispersion of magnetic nanoparticles was prepared by the addition of an aqueous mixture of ferric and ferrous salts to a strong alkaline solution (NaOH or NH_4OH) at room temperature. In the present study, a solution of NaOH was used as alkali source instead of ammonia. Oxygen is eliminated from the solution by using N_2 gas flow through the reaction medium in a closed system during the synthesis operation.

SPION with average particle size of 6 nm were prepared without any additional stabilizer according to the following procedure. Typically, 5 mL of iron solution with containing 0.1 M Fe^{2+} and 0.2 M Fe^{3+} is added dropwise into 50 mL of alkali solution (NaOH) under vigorous mechanical stirring (2000 min^{-1}) for 30 min at room temperature. Color of the suspension turned to black almost immediately. SPION with particle size of 12 nm was prepared by increasing the reaction temperature. All the procedures and experimental conditions were the same as those for the synthesis of 6-nm SPION, except the alkaline solution was preheated to 80 °C before the coprecipitation reaction. The precipitated powders were collected and removed from the solution by applying an external magnetic field. The supernatant solution was removed from the precipitate after decantation. Deoxygenated Milli-Q water was added to wash the powder, and the solution was decanted after centrifugation at 3500 min^{-1}. After washing the powder 4×, 1×10^{-2} M HCl solution was added to neutralize the anionic charge on the surface of the particles. The positively charged colloidal particles were then separated by centrifugation and peptized by adding deoxygenated Milli-Q water. Using XRD measurements, Fe_3O_4 nanoparticles of 12-nm size were selected for the further coating process. Three different types of magnetic colloids were prepared according to the following procedures.

(a) NaOl Modified SPION. A 15-mg aliquot of NaOl was added to 50 mL (1.1 mg/mL) of SPION suspension. The solution was dispersed with strong sonication for 5 min, during which the suspension was heated to about 80 °C as a result of the strong hydrodynamic force, and then cooled to room temperature. The degree of coating was evaluated by ξ-potential measurements at about pH 7 with electrokinetic sonic amplitude (ESA).

(b) MPEG-Modified SPION. The SPION suspension was washed several times with analytical grade methanol (99.5%) with a help of a strong external magnet. An aliquot of 5 mL with a concentration of 10 mg/mL SPION was dispersed in toluene/methanol (1:1 v/v) mixture and heated at 95 °C under N_2 until 50 vol % of the solution was evaporated. After evaporation, methanol was added in equal volume and the mixture was re-evaporated to one-half. This procedure was repeated 3× until residual water was thoroughly removed. A solution of 3-aminopropyltrimethoxy silane (APTMS) was added to the suspension. APTMS acts as a coupling agent, where silanization takes place on the particle surfaces bearing hydroxyl groups in the organic solvent. This results in formation of a three-dimensional polysiloxane network. The ferrofluid suspension was stirred and heated under N_2 atmosphere at 110 °C for 12 h. The silanization taking place during the reflux of APTMS results in the formation of APTMS coating with a thickness of two or three molecular layers, tightly cross-linked with a large surface density of amines. Afterward, the silanized SPION were subsequently sonicated for 2 min in a mixture of toluene/methanol (1:1 v/v). After cooling the solution temperature to 80 °C, 50 mg of MPEG 5000 was added to coat the surface of the SPION.

Chemical bonding information on metal−oxygen, hydroxyl, and other functional groups was obtained with Fourier transform infrared spectroscopy (FTIR, Avatar 360, Nicolet) using

(23) Kim, D. K.; Toprak, M.; Mikhaylova, M.; Zhang, Y.; Bjelke, B.; Kehr, J.; Muhammed, M. Nanoparticulate Materials. *Mater. Res. Soc. Symp. Proc.* **2002**, *704*, 369.

the Smart DuraSamplIR Diamond ATR Accessory. Each spectrum was collected after 32 scans at a resolution of 1 cm^{-1}.

For AFM imaging of MPEG-coated SPION, a silicon wafer was used as the substrate. The silicon wafer was cut into pieces of 1 × 1 cm. These wafers were washed with acetone first and N_2 was blown for drying. Piranha solution was used to degrease and de-oxygenate the substrate surface. The dried wafers were then silanized in the following way. The silicon pieces were placed on a hot plate in a vacuum chamber. On the plate was also a small three-neck flask loaded with 200 μL of APTMS in 20 mL of toluene. In low vacuum, the hot plate was heated to 60 °C for 10 min to saturate the silicon substrate with the solution. The temperature was then increased to 150 °C for 1 h to form the silane molecules on the silicon surface. The silanized silicon was immersed in MPEG-coated SPION suspension for 10 min, rinsed in deionized water, and blown dry by N_2.

(c) Starch-Modified SPION. Starch (100 mg) was dissolved in 20 mL of distilled and deionized water at 80 °C under magnetic stirring. A 5-mL portion of solution containing 0.1 M Fe^{2+} and 0.2 M Fe^{3+} was poured into a prepared starch solution under vigorous stirring. The starch and iron ion mixture (25 mL) was then added dropwise into 250 mL of 0.1 M NaOH under vigorous mechanical stirring (2000 min^{-1}) at 60 °C for 2 h. Around 50 wt % of water was evaporated, and the remaining solution was cooled to room temperature and allowed to stand 12 h. The gels formed were washed with deionized water until the pH became less than 8.5. Excess salt and ions were removed by using dialysis at 37 °C for 2−3 days against 5 L of distilled water. To cleave glycosidic bond and reduce the polymeric chain to an average molecular weight, the influence of oxidizing agent, used for cleavage of the polymeric starch chains, was investigated. H_2O_2 (5 mL of 0.46 M) was mixed with 20 mL (10 mg/mL) of starch-coated SPION.

3. Characterization. The structure of the precipitated powders was obtained by X-ray powder diffraction (XRD) with a Philips PW 1830 diffractometer, using a monochromatized X-ray beam with nickel-filtered Cu Kα radiation. The average size of the crystals (D; nm) was estimated using Scherrer's formula.[24] A TEM study was carried out using a JEOL-2000EX microscope. The particle size distribution was measured using a Brookhaven BI-XDC by measuring the rates of sedimentation under applied centrifugal force based on X-ray absorption and BI-90 particle sizer based on dynamic light scattering (DLS). The surface morphology was examined by atomic force microscopy (AFM). An AFM Nanoscope IIIa system was used in the tapping mode by employing a silicon tip with a resonance frequency in the range 286−313 kHz.

The ξ-potential of the powder suspension was measured in 5×10^{-3} M and 1×10^{-2} M NaCl background electrolyte solutions using a Zetasizer 2000 (Malvern Instrument Ltd.). The test suspension was prepared at a fixed concentration and a set of predetermined pH values were adjusted using NaOH or HCl stock solutions.

In situ monitoring of NaOl-coated SPION was carried out by ESA-9800 (Matec Applied Sciences). In this technique, the dynamic mobility, also called the acoustic pressure amplitude (ESA), was generated by colloidal particles in alternating high-frequency electric fields.

$$ESA = c \times \Delta\rho \times \Phi \times \mu(\omega) \tag{4}$$

where c is the sound velocity in the dispersing liquid, $\Delta\rho$ is the difference between the solid and liquid density, Φ is the volume fraction of solid in the dispersion, and μ is the dynamic mobility. The dynamic mobility is calculated from the following equation:

$$\mu = \frac{2\xi\epsilon}{3\eta} G[1 + \gamma F(\kappa a)] \tag{5}$$

where ξ is the zeta potential, ϵ is the dielectric constant of the medium, and γ is an inertial term that is a function of the amplitude and phase of the acoustic signal. G is a geometrical factor for a given electrode geometry and is a constant for a set of experiments. The term in brackets contains γ, which depends on the conductivities of the solution and of the particles, and the function $F(\kappa\alpha)$, where κ is the reciprocal of the Debye length and α is the curvature radius of the double layer.

Mössbauer spectra were measured with a conventional transmission Mössbauer spectrometer operating in constant acceleration mode ($T = 300$ K). The Mössbauer spectrum gives information on the oxidation state of iron, even though vacancies may exist in the crystal structure. A ∼100 mCi of ^{57}Co(Rh) source was used and the spectrometer was calibrated using α-iron at room temperature.

The magnetization of the samples was measured with a 7 T Quantum Design SQUID magnetometer between 5 and 300 K. For zero-field cooled (ZFC) experiments, the sample was cooled and a constant field was applied during the warm scan.

Results and Discussion

1. Thermodynamic Modeling. The synthesis of magnetite has been studied and reported by several other groups. However, it is essential to synthesize magnetite as a pure phase and with controlled particle size and shape. In the present study, SPION with particle size in the order of 10−12 nm was targeted to satisfy its use for biomedical purposes. When the particle size is larger than the superparamagnetic size limit, the magnetite shows ferromagnetic behaviors.

The synthesis of SPION has been performed using a solution chemical method. The synthesis of magnetite is reported in several studies using several different techniques including coprecipitation. In most of these reports, however, the experimental conditions have been reached through a "trial and error" approach, with little consideration for theoretical basis of the solution chemistry of the reaction system.

A rational approach has been adopted to synthesize a pure phase of magnetite based on the quantitative analysis of different reaction equilibria involved in the precipitation of magnetite from aqueous solutions. The thermodynamic modeling of the chemical system for the coprecipitation of magnetite phase from aqueous solutions containing suitable salts of Fe^{2+} and Fe^{3+} has been performed. The results of the thermodynamic modeling, together with available kinetic information of relevant reactions, have been used for the selection of the optimum experimental conditions for the synthesis of magnetite from aqueous solutions. In this way it is possible to establish, on a rational basis, the chemical conditions (including the composition of the reaction media, pH, redox potential, concentration of the different salts used, etc.) as well as the boundary conditions in which magnetite could be formed reproducibly as a pure phase.

Thermodynamic modeling of the different phase formation under closed system and/or surrounding conditions can be calculated from the changes of the free energy, ΔG, of the reaction under given conditions. Iron exists in three oxidation states and therefore redox reactions must be taken in consideration. The formation of the different iron species is correlated through different redox reactions.

(24) Massart, R.; Cabuil, V. *J. Phys. Chem.* **1987**, *84*, 967.

$$Fe^{3+} + e^- \rightarrow Fe^{2+} \quad \text{and} \quad Fe^{2+} + 2\,e^- \rightarrow Fe_{(s)} \qquad (6)$$

Magnetite can be obtained by controlled oxidation of Fe^{2+} in solution according to the following equations:

$$3\,Fe^{2+} + 4\,H_2O \rightarrow Fe_3O_4 + 6\,H^+ + 6\,H_2 \qquad (7)$$

$$Fe^{2+} + O_2 + OH^- \rightarrow Fe_3O_4 + H^+ \qquad (8)$$

However, the kinetics for the oxidation of Fe^{2+} is slow and difficult to control. It is therefore more practical to control the formation of magnetite through the use of a mixture of Fe^{2+} and Fe^{3+} in the start solutions. In this case, the oxidation of Fe^{2+} should be avoided.

In the thermodynamic modeling of the precipitation of the magnetite we define the system to be investigated by the following main components:

$$Fe^{2+}, Fe^{3+} - (NO_3, Cl) - H_2O \qquad (9)$$

Chloride and nitrate ions are considered separately in order to study the effect of the ligand on the formation of magnetite. A plot of the concentration of the reaction products of all possible chemical reactions that can take place in the system is given in Figure 2. As shown, Fe_3O_4 can be formed over a wide pH range for given concentrations of Fe^{2+} and Fe^{3+}. This plot is complicated and we therefore consider the system in more simplified way.

Figure 3 shows the thermodynamic modeling of Fe^{2+}–Cl^- system at pH 12. At pH 12, Fe_3O_4(s) forms in a redox potential range of $E = -0.34$ to -0.85 V (SHE), and it oxidizes into FeOOH(s) at $E > -0.4$ V (SHE) but reduces to metallic iron at $E < -0.85$.

Figure 4 (a) and (b) show the results of another set of calculations, where we kept the stoichiometric ratio of $Fe^{2+}/Fe^{3+} = 1{:}2$. As shown, Fe^{2+} and Fe^{3+} ions form week complexes with Cl^- ions that appear only in the acidic pH range. Fe_3O_4(s) is formed in a relatively wide pH range of 4−14. However, it is noticed that by increasing the solution pH, Fe^{3+} forms a stable solid precipitate of FeOOH(s) in the pH range of 1−4. Although Fe_3O_4 is thermodynamically stable at higher pH, the transformation of FeOOH(s) to Fe_3O_4(s) is known to be kinetically slow. From these calculations it can be suggested that pure magnetite phase can be synthesized by adding solution containing ferrous and ferric chloride in 1:2 molar ratio to a strong alkali solution, e.g., NaOH or NH_4OH. A suitable redox potential should be maintained, about +0.4 V (SHE) which is controlled by the ratio of $[Fe^{2+}]/[Fe^{3+}]$. At higher oxidation potential, Fe^{2+} will be oxidized to Fe^{3+} and magnetite cannot be obtained as a pure phase. It should be noted that these calculations are performed on equilibrium data at 25 °C. The numerical values for these reactions at higher temperatures are not readily available. We therefore used these results as indication for the synthesis conditions which are expected to be valid also at higher temperature (80−90 °C)

2. Colloidal Processing. Colloidal processing of magnetic nanoparticles has been extensively studied with the emphasis on the characteristics of SPION dispersion as a ferrofluid. Suspensions of SPION have van der Waals' forces and magnetic dipole−dipole

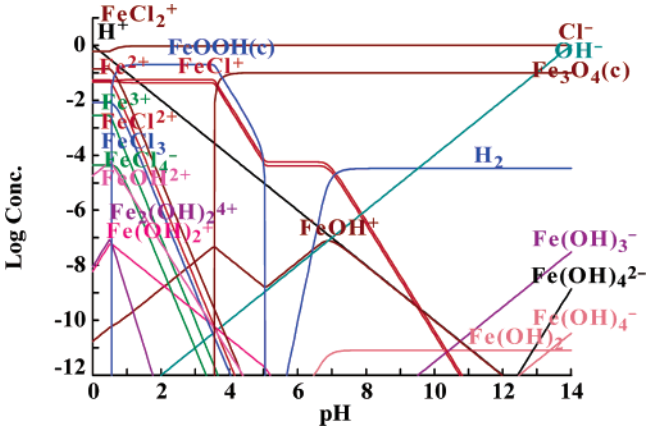

Figure 2. Thermodynamic calculations of the concentrations of all Fe^{2+} and Fe^{3+} species formed at different solution pHs. Initial conditions are $[Fe^{2+}] = 0.1$ M, $[Fe^{3+}] = 0.2$ M, and $[Cl^-] = 1.0$ M.

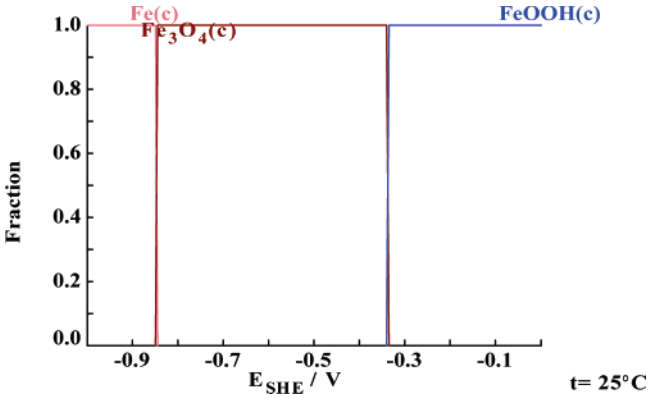

Figure 3. Thermodynamic modeling diagram showing the distribution of the fraction of $[Fe^{2+}]/[Fe^{2+} + Fe^{3+}]$ vs the redox potential (E at standard hydrogen electrode) calculated at 25 °C for 0.3 M $FeCl_2$ solution at pH 12.

interactions generated from residual magnetic moments, which tend to agglomerate and flocculate the particles.

Ferrofluids composed of SPION are not only affected by an inhomogeneous particle size distribution, but also by the surface charge of the particles in the solution. One of the practical methods to stabilize the ferrofluids is through electrostatic repulsion forces, achieved by similar surface charge. The repulsive force results from the formation of an electrical double layer around the particles, which strongly affects the dispersion of the particles into a polar media, and is dependent on several factors including pH, particle concentration, and ionic strength of the suspension. A colloidal solution is a suspension in which the dispersed phase is so small that gravitational forces are negligible and particles' interactions are dominated by short-range forces, such as van der Waals' attraction, and surface charges. The inertia of the dispersed phase is small enough that it exhibits Brownian motion, a random walk driven by momentum transferred through collisions with molecules of the suspending medium.[25]

Ferrofluid consists of monodomain SPION, which can be considered as point dipoles with a magnetic moment ($m = (\pi/6)M_s d_m^3$). The dipole−dipole interaction (m_1 and

(25) Khalafalla, S. E.; Reimers, G. W. U.S. Patent 3764540, 1973.

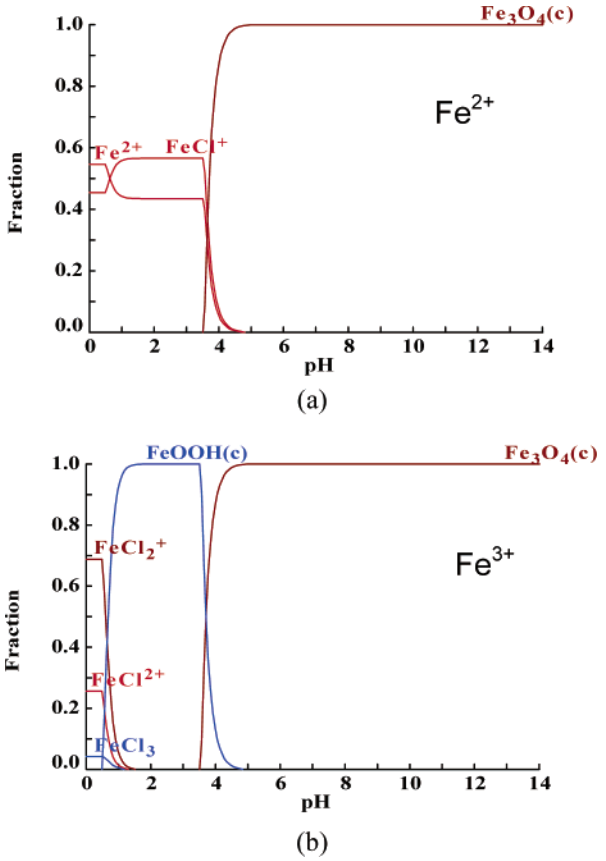

Figure 4. Thermodynamic modeling diagram showing the distributions of the fraction of $[Fe^{X+}]/[Fe^{2+}+ Fe^{3+}]$ vs pH calculated at 25 °C for 0.1 M $FeCl_2$ and 0.2 M $FeCl_3$ solution at pH 12: (a) $[Fe^{2+}]$ vs pH, and (b) $[Fe^{3+}]$ vs pH.

m_2) between the single magnetite nanoparticles at a distance r_{12} is

$$U_{dd} = \frac{\mu_0 m_1 m_2}{4\pi r_{12}^3}[\hat{m}_1 \times \hat{m}_2 - 3(\hat{m}_1 \times \hat{r}_{12})(\hat{m}_2 \times \hat{r}_{12})] \quad (10)$$

where the symbol "∧" denotes a unit vector. In an energetically ideal condition, the magnetic moments are aligned in the same direction.

The van der Waals attraction force between the SPION cores can be expressed by

$$U_{VDW} = -\frac{A}{12}\left[\frac{1}{S^2-1} + \frac{1}{S^2} + 2\ln\left(\frac{S^2-1}{S^2}\right)\right] \quad (11)$$

where A is the Hamaker constant (approximately 4×10^{-20} J for magnetite in water)[26] and $S = r_{12}/d$.

The SPION are usually grafted with nonmagnetic substances to form a stable ferrofluid. From eqs 10 and 11, it is evident that the interactions between particles are mainly dominated by dipole interactions when the coating thickness is more than 2 nm. For coating thickness less than 2 nm, the dipole−dipole interaction is larger than the van der Waals interaction. However, it should be noted that the van der Waals force is much stronger than the values that can be estimated by eq 11.[27]

The crystal structure of natural and synthetic magnetite is octahedral. Magnetite nanoparticles obtained by precipitation methods (from solutions at temperatures lower than the boiling point of the reaction mixture) may be round in shape. Figure 5 shows a TEM image and size distributions of dried SPION taken from the corresponding colloidal particles prepared at different temperatures. Spherical or ellipsoidal particles with the characteristic crystalline order of magnetite and diameters around 5.7 and 12 nm were observed. Usually, spherical shapes are formed because the nucleation rate per unit area is isotopic at the interface between the SPION. The size distribution was calculated based on a log-normal function and image analysis program.

The particle sizes determined by the equation were 5.7 and 12 nm which agree well with the crystal sizes calculated from XRD data (6 and 12 nm) given in Figure 6. Therefore, the reaction temperature during the synthesis of magnetite has a significant effect on the particle nucleation, subsequent growth, and crystallinty. XRD patterns of the chemically prepared small magnetite nanoparticle (size ∼6 nm) and coated samples have shown very low crystallinty and therefore are not suitable for accurate phase analysis.

The Mössbauer spectrum of Fe_3O_4 was measured (Figure 7) and was found to be composed of two sextets corresponding to two kinds of Fe sites in the spinel structure having the following arrangement: $[Fe^{3+}]_{(A)}$-$[Fe^{3+}Fe^{2+}]_{(B)}$. The outer sextet corresponds to the tetrahedral A-site $[Fe^{3+}]$ and the inner sextet corresponds to the octahedral B-site $[Fe^{2+}$ and $Fe^{3+}]$. Their internal fields were calculated as 491 and 453 kG, respectively, at room temperature. Nonstoichiometric $Fe_{3-\delta}O_4$ can be written as $[Fe^{3+}]_{(A)}[Fe_{1+2\delta}{}^{3+}Fe_{1-3\delta}{}^{2+}X_\delta]_{(B)}$, where X stands for vacancy. Following the pair model or the local charge compensation model, it is possible to rewrite this as $[Fe^{3+}]_{(A)}[Fe_{2-6\delta}{}^{2.5+}]_{(B)}[Fe_{5\delta}{}^{3+}X_\delta]_{(B)}$ when rapid electron hopping process takes place between Fe^{2+} and Fe^{3+} ions in the octahedral B sites, resulting in average charged $Fe^{2.5+}$ ions. Nonstoichiometric magnetite, $Fe_{3-\delta}O_4$, is obtained as a result of the oxidation of ferrous ions to ferric ions. Excess Fe^{2+} ions in nonstoichiometric phases are oxidized to Fe^{3+} in order to compensate for the extra charge of randomly distributed vacancies in octahedral B-sites.[28]

Mössbauer spectra of uncoated SPION may be attributed to one doublet and one sextet (the areas of the components are in the ratio 34.2:65.8%), i.e., $^1/_3$ of the particles are in the superparamagnetic (SPM) state during the recording of the spectrum ($T = 300$ K $> T_B$). The value of isomer shift remains almost constant when applying a magnetic field, while at zero field the obtained values correspond to that of magnetite. However, the value of H_{eff} for an applied magnetic field corresponds to changes in site occupations of the magnetic sublattice, possibly by transference of electron density. This can be caused by the electron hopping process between Fe^{2+} and Fe^{3+} cations in the Fe_3O_4 crystallites. Actually, the character of Mössbauer spectra corresponds to particles with size between 3 and 10 nm. The line broadening of the sextet is due to the distribution of different particle sizes and the various

(26) Scholten, P. *J. Magn. Magn. Mater.* **1983**, *39*, 99.
(27) Ewijk, G. A. V. Ph.D. Thesis, Universiteit Utrecht, Nederlands, 2001.
(28) Greenwood, N. N., Gibb, T. C., Eds. *Mössbauer Spectroscopy*; Chapman and Hall: London, 1971; p 251.

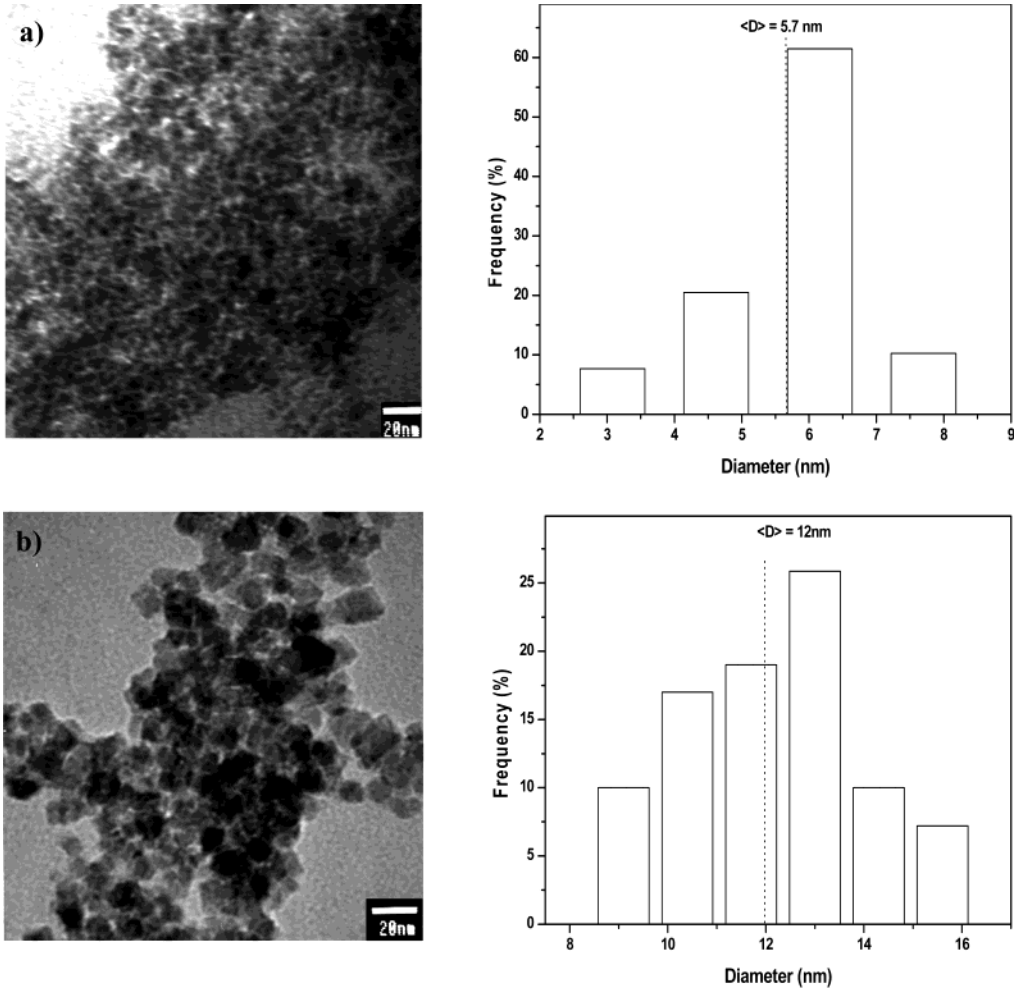

Figure 5. Electron microscopy images (left) and the corresponding particle size histograms (right) of uncoated magnetite nanoparticles prepared by controlled coprecipitation: (a) at room temperature, and (b) after heat treatment (the reaction mixture was heated at 80 °C for 1 h).

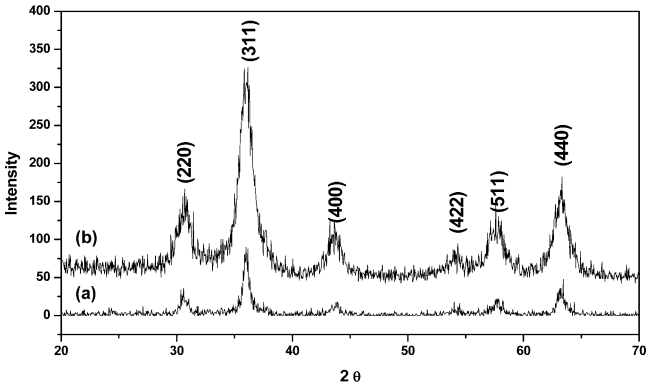

Figure 6. X-ray powder diffraction patterns for uncoated magnetite nanoparticles prepared by controlled coprecipitation: (a) at room temperature, and (b) after heat treatment (the reaction mixture was heated at 80 °C for 1 h).

types of crystallographic surrounding of each iron atom. A quadrupole component (doublet) is assigned to SPM fraction. These components disappear when a magnetic field is applied and the state of all magnetic particles becomes nonsuperparamagnetic state.

Figure 8 shows a TEM image of starch-coated SPION that can be used to determine the real particle size distribution and morphology. Spherical or ellipsoidal particles consisting of a SPION core with a diameter around 6 nm were found. However, it is evident that the SPION were distributed homogeneously in the polymeric matrix. Spherical shapes are formed because the nucleation speed per unit area is isotopic at the interface between the SPION. The results of the DLS size analysis and TEM images showed that the observed size distribution is for the agglomerated clusters rather than the individual particles. The average cluster size for starch-coated SPION measured by DLS showed 42 nm by the addition of 5 mL of 0.46 M H_2O_2. The SPION produced in a starch matrix showed extremely stable behaviors for 1 year in aqueous media at room temperature.

Figure 9 shows an AFM image of MPEG-immobilized SPION and its section analysis results. As shown, each cluster includes several magnetite single particles with the cluster size around 120 nm.

The magnetic hysteresis loop measurement from 5 to 300 K for the MPEG-coated SPION is shown in Figure 10. The typical characteristics of superparamagnetic behavior are observed by showing almost immeasurable coercivity and remanence above the blocking temperature. The SPION are ferri- or ferromagnetic single-domain particles that have significantly small thermal energy with the same order of magnitude as the anisotropy energy barrier.

The magnetic particle size has been calculated using room-temperature magnetization data. A model for

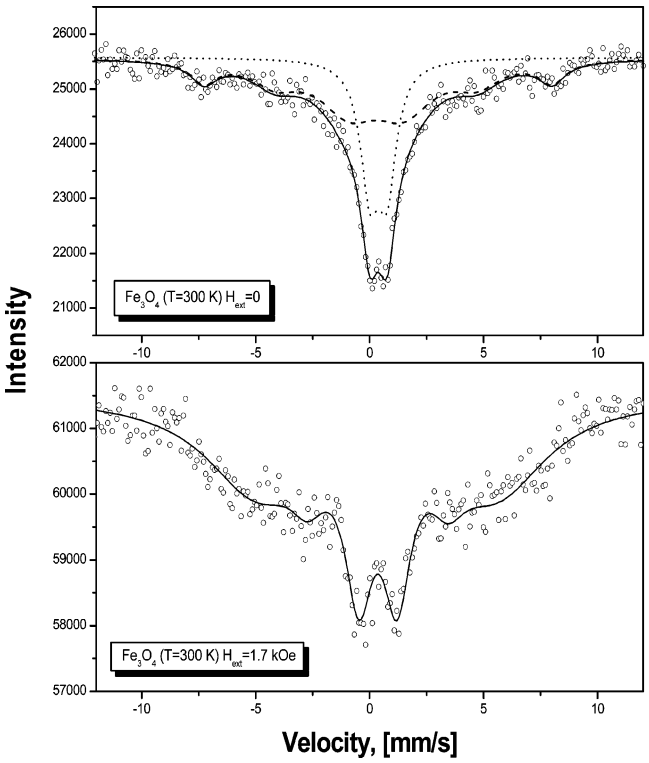

Figure 7. Mössbauer spectrum of uncoated Fe_3O_4 in the presence and absence of external magnetic field (H_{ext} = 1.7 KOe).

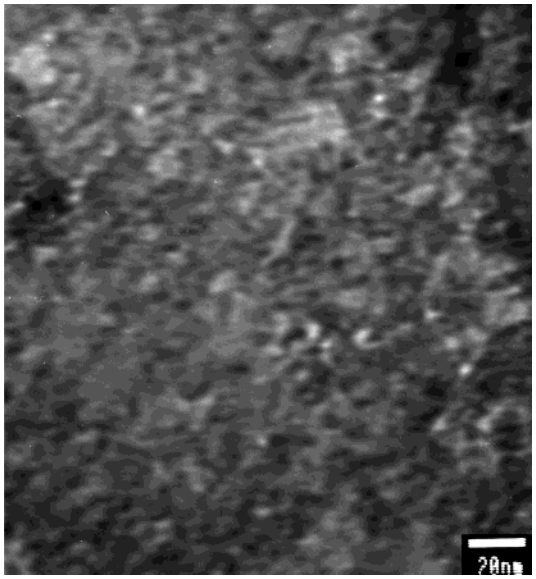

Figure 8. Electron microscopy image of starch-coated SPION. TEM shows the random particle distribution of SPION in polymeric starch matrix.

monodomain, noninteracting particle was used for this calculation. Using the initial susceptibility χ_i and the bulk saturation magnetization of the particle per unit volume M_s, the mean volume diameter D_v of the log-normal volume distribution can be calculated by

$$D_v = \left(\frac{18k_BT}{\pi M_s}\sqrt{\frac{\chi_i}{3\epsilon M_s H_0}}\right)^{1/3} \qquad (12)$$

where $^1/_{H_0}$ is the point where the high-field linear extrapolation of M versus $^1/_H$ crossed the abscissa, and

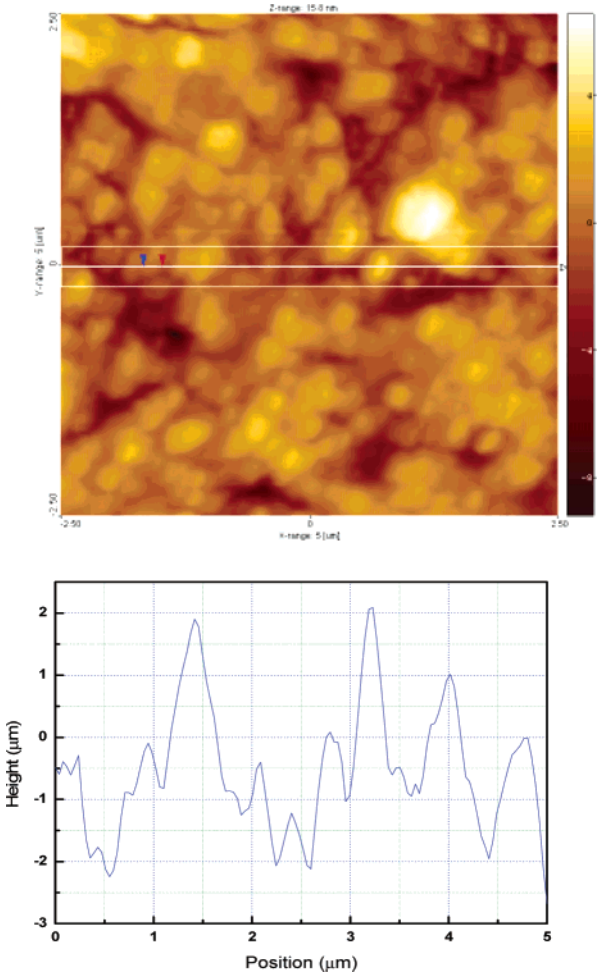

Figure 9. AFM image of MPEG-coated magnetite and section analysis results.

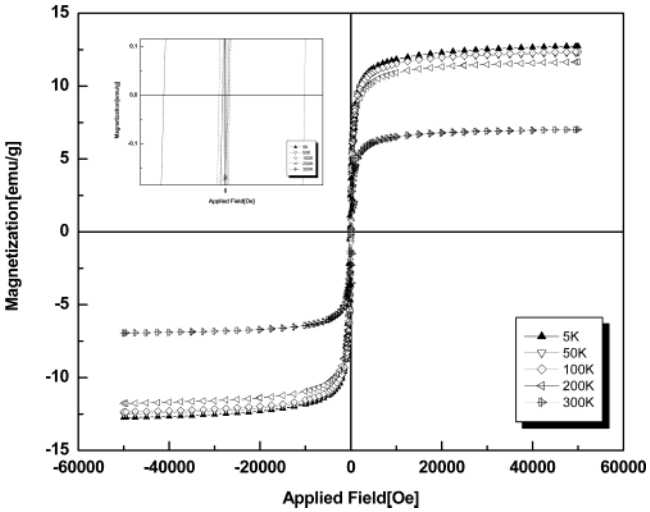

Figure 10. Magnetization vs applied magnetic field for MPEG-coated SPION.

ϵ is the particle volume fraction. A magnetic core diameter of 5.2 nm was obtained from magnetization measurements. Differences between the particle size determined by TEM and that determined by magnetization measurements can be attributed to several factors. First, a magnetically dead layer on the surface decreases the uniformity due to quenching of surface moments. Second, some of the iron species exist as a nonmagnetic amorphous phase, which does not contribute to the

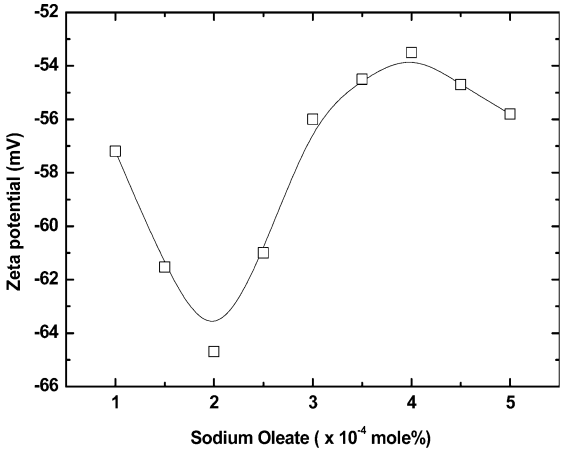

(a)

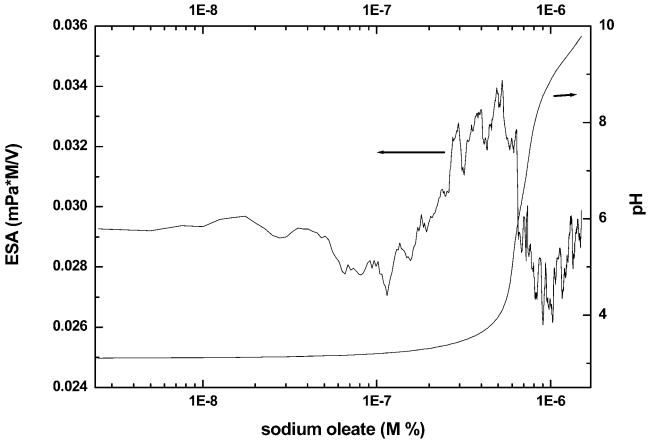

(b)

Figure 11. (a) ξ-Potential measurements of SPION suspensions containing different concentrations of NaOl at pH 7; and (b) variation of the pH and ESA of SPION suspensions containing different concentrations of NaOl.

magnetic behavior, or as an iron phase that will have a smaller effect on magnetization than a magnetite only phase. Third, the amount of MPEG at SPION surface was not taken into account during the calculations.[22]

Agglomeration of the magnetite particles is initiated from collisions between the particles during nucleus formation. The collision of particles forms initial agglomerated clusters in the liquid carrier. Growth of the agglomerate takes place by attraction forces and capillary forces between magnetite clusters and single particles. The cluster size increases until the forces balance between the clusters and equilibrium is reached. Nanosized magnetite particles have large surface area and small curvature. This large surface energy accelerates the agglomeration process in order to decrease the free energy (ΔG) of the system.

To avoid precipitation of SPION, the stabilization is introduced against aggregation and flocculation usually using organic surfactant compounds such as NaOl. Figure 11 a shows the results of ξ-potential measurements of SPION as a function of NaOl concentrations at pH = 7. At NaOl concentration of 2×10^{-4} M ξ-potential showed a maximum value, and then the ξ-potential decreased when more than 2×10^{-4} M NaOl

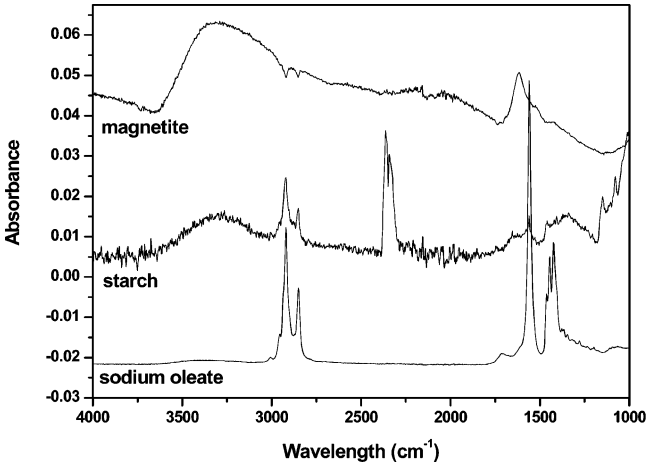

Figure 12. FTIR spectra of magnetite, cationic potato-starch-coated SPION, and anionic NaOl-coated SPION.

was added. This can be the result of NaOl forming as a monolayer on the SPION surface at 2×10^{-4} M, and therefore it shows a maximum value of ξ-potential. For concentration of NaOl less than 2×10^{-4} M, the amount of NaOl is not enough to form a compact film on the surface of SPION.

By increasing the thickness of the NaOl coating layer by adding an excess amount of NaOl, the ξ-potential value starts to decrease again due to strong interaction between NaOl molecules. The adsorbed NaOl interacts with surface Fe−OH groups to form iron complexes, which results in the modification of the surface charge properties. From the ξ-potential measurements, the optimum amount of NaOl for the coating on SPION can be determined.

Compared to the ESA measurement shown in Figure 11b, traditional measurements of particle size and ξ-potential usually involve light scattering or sedimentation techniques and require a very high degree of dilution of the colloidal suspension used. This dilution often changes both the particle size distribution and the ξ-potential of the sample. Therefore, characterization studies made on the concentrated sample directly without dilution allow realistic evaluation of the true agglomeration status of the colloid and hence optimization of the dosage of various chemical additives. Different from conventional methods for measuring ξ-potential, acoustic spectroscopy can provide accurate ξ-potential data even in concentrated slurries.

The variation of pH of the suspension and the concentration of NaOl were studied to determine the maximum adsorption to form NaOl monolayer on SPION surfaces by ESA measurements. Figure 11b shows the results of in situ ESA measurements obtained at different amounts of NaOl adsorption on SPION surface. An aliquot of 250 mL (10 mg/mL) SPION suspension at pH 3 was placed in a Teflon sample container. NaOl (100 μL of 1×10^{-3} M) was added by a Microlab 500 digital buret and the suspension was left for 10 s to stabilize before the measurements were taken. The electro-acoustic signal, electrical conductivity, and temperature were monitored as a function of pH during the NaOl titration. The stirring speed was maintained constant at 1200 min^{-1}. When the NaOl was added at pH 3, the ESA values decreased until reaching 0.027 mPa·M/V at 1.1×10^{-7} M NaOl. At 5.2×10^{-7} M NaOl

Table 1. Hyperfine Parameters of the SPION, MPEG-Coated SPION, and Starch-Coated SPION With and Without Magnetic Field for the Mössbauer Spectrum at 300 K

sample			*S* (%)	*d* (mm/s)	*G* (mm/s)	Q. S. (ΔE_Q) (mm/s)	H_{eff} (kOe)
SPION	doublet	1	34.2	0.38 ± 0.014	0.992 ± 0.083	0.755 ± 0.029	
($H_{ext} = 0$)	sextet	1	65.8	0.321 ± 0.057	1.355 ± 0.337	−0.071 ± 0.103	474.432 ± 0.173
		2			2.475 ± 0.6487		
		3			3.198 ± 0.517		
SPION	sextet	1	100	0.332 ± 0.047	5.466 ± 0.665	0.056 ± 0.080	328.742
($H_{ext} = 1.7$ KOe)		2			1.899 ± 0.425		
		3			1.483 ± 0.104		
SPION + MPEG	singlet	1	31.7	0.765 ± 0.046	3.142 ± 0.286		
($H_{ext} = 0$)	sextet	1	68.3	0.691 ± 0.0067	2.172 ± 0.441	−0.067 ± 0.094	425.29
		2			3.063 ± 0.610		
		3			4.243 ± 1.904		
SPION + MPEG	sextet	1	52.5	0.714 ± 0.039	1.216 ± 0.148	0.004 ± 0.078	451.32
($H_{ext} = 1.7$ KOe)		2			1.272 ± 5.755		
		3			1.111 ± 0.423		
	sextet	1	47.5	0.533 ± 0.130	1.043 ± 0.257	−0.273 ± 0.252	369.817
		2			1.166 ± 3.049		
		3			3.261 ± 1.644		
SPION + starch	doublet	1	100	0.387 ± 0.004	0.617 ± 0.011	0.712 ± 0.07	
($H_{ext} = 0$)							

the maximum ESA occurs with a value of 0.034 mPa·M/V. The pH of the suspension also gradually increases as the concentration of NaOl in the suspension increases. This is because NaOl can be transformed to oleic acid, at strong acidic region, which is the dominant adsorbed species at the SPION surface. On the other hand, the pH of the suspension was found to be between 4 and 8.7. It appears that NaOl and oleic acid interact through the formation of hydrogen bonds between the fatty acid (carboxylic acid) and the surfactant (carboxylate ion). This results in a decrease in the ESA values from 0.034 mPa·M/V to 0.0026 mPa·M/V. As the concentration of NaOl increases to more than 1×10^{-6} M (pH ≥8.7), the dominant species in the suspension is NaOl resulting in a slight increase in ESA value. However, when excess NaOl is added to the SPION suspension, the particles show more flocculation and precipitation than in the absence of NaOl.

The chemisorption of NaOl at SPION surfaces changes the interfacial properties between the magnetite colloidal nanoparticles and the solvent. Thus, by properly adjusting the pH and the ratio between SPION and the amount of NaOl in suspension, the environmental conditions for the formation of a stable ferrofluid can be optimized by using in-situ monitoring of ESA values.

Figure 12 shows FTIR spectra of magnetite, anionic NaOl-coated SPION, and cationic potato-starch-coated SPION collected from the solid sample using the Smart DuraSamplIR Diamond ATR accessory. In the case of NaOl, the band at 1530−70 cm^{-1} is originated from the NaOl in coating layer (COO^- stretching of oleate). The band at 2919 cm^{-1} is originated from the CH_2 group. Compared with the reported position of the asymmetric $-COO^-$ stretching vibration of pure NaOl at 1563 cm^{-1}, the attachment of the coating gel onto the SPION surface induces a shift of that asymmetric $-COO^-$ stretching, which occurs at 1560 cm^{-1}. FTIR measurements show that there is a strong interaction between the C═C bond of adsorbed NaOl molecule and the surface of SPION, because of interaction between the carbonyl group and the base during the stabilizing process. It is also well-known that the interaction of NaOl with colloidal magnetite leads to the formation of ferric oleate. In the case of starch-coated SPION, the band at 3381 cm^{-1} is originated from the O−H stretching, the band at 2931 cm^{-1} is originated from the C−H

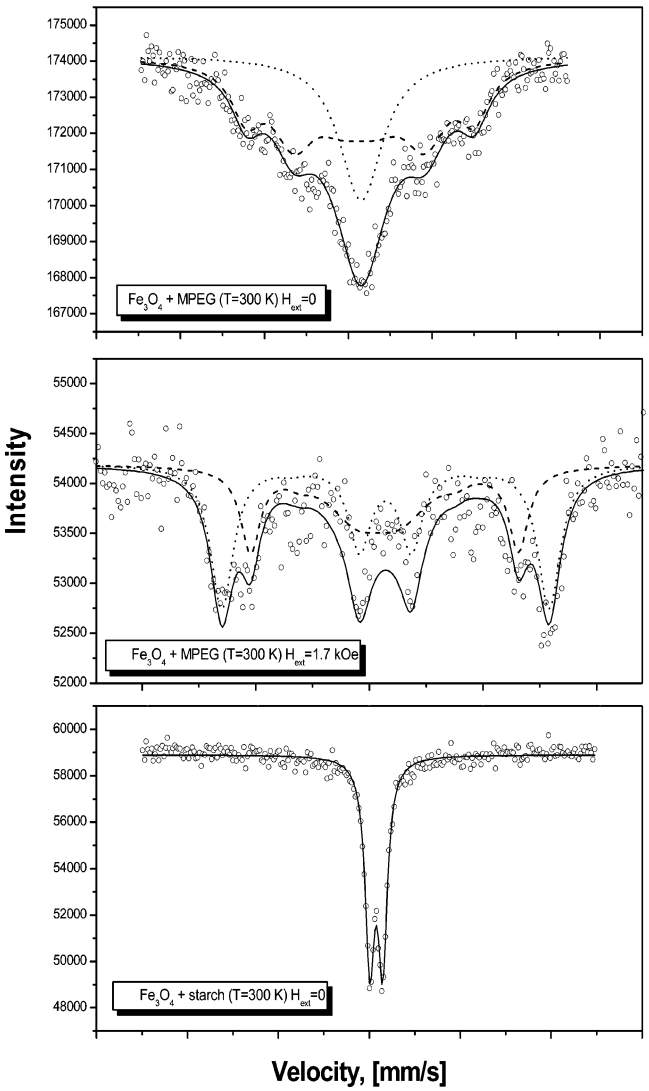

Figure 13. Mössbauer spectrum of MPEG-coated Fe_3O_4 with and without external magnetic field, and starch-coated Fe_3O_4 without magnetic field.

stretching, the band at 1652 cm^{-1} is originated from the C═C stretching, the band at 1420 cm^{-1} is originated from the C−H bending, and the band at 1054 cm^{-1} is originated from the C−O−C bending.

Table 1 shows hyperfine parameters of the SPION, starch-coated SPION, and MPEG-coated SPION with and without magnetic field for the Mössbauer spectrum at 300 K. In this experiment, only one broad line sextet was observed, which is not in a agreement with bulk Fe_3O_4 spectra. This suggests that two distorted magnetic sublattices are not well resolved in an ultra dispersion state.

The Mössbauer spectra for SPION coated with starch and MPEG were also measured. Figure 13 shows that for starch-coated SPION, a total transformation to the SPM state is observed in contrast to the MPEG-coated SPION. The value of isomer shift remains almost constant in comparison with that of uncoated SPION. A distinctive peculiarity of SPION coated with MPEG is observed in the exhibition of a very broad line spectrum so that a doublet, which is observed for uncoated SPION, is registered as a singlet even though the correlation between spectral areas remains almost constant. The isomer shift also increases for the MPEG-coated SPION, under both applied magnetic field and zero-field conditions, because the process of electron density transfer takes place in both cases. It should be noted that the applied magnetic field results in a transformation of one of the spectral components (singlet) to a sextet suggesting that a fraction of the SPM particles become ferrimagnetic. The existence of a diamagnetic coating prevents the interaction of particles, leading to the averages of the H_{eff} values.

Conclusions

Superparamagnetic iron oxide nanoparticles (SPION) with diameters of 6 and 12 nm have been prepared by controlled chemical coprecipitation which was guided by chemical equilibrium calculations of Fe−Cl−H_2O system. Undesired critical oxidation of SPION was protected by the use of nitrogen atmosphere during the synthesis. Three different types of magnetic colloids have been prepared by using biocompatible coating agents MPEG, starch, and NaOl, which are stabilized through various methods. Many kinds of biological substancs are hydrophilic and water soluble, so they cannot pass through the hydrophobic lipid bilayer membranes. This is because MPEG has been coated at the SPION surface to produce uncharged hydrophilic residues and very high surface mobility leading to high steric exclusion. Therefore, it is expected to effectively improve the biocompatibility of the nanoparticles and to possibly prevent accumulation in RES or mononuclear phagocyte systems (MPS).

From the Mössbauer spectra, coating of the SPION with starch is more favorable because all the particles are transformed to SPM states. However, starch-coated SPION seems to change the electron structure of the SPM particle to a lesser extent.

Acknowledgment. This work has been supported by Swedish Foundation for Strategic Research (SSF). We specially thank Prof. N. Bobrysheva, Prof. M. Osmolowsky, and Prof. V. Semenov from Saint-Petersburg State University for Mössbauer measurements, and Dr. Sang Ho Yun and Prof. Judy Wu from University of Kansas for SQUID measurements.

CM021349J